ATOMIC PHYSICS

Thermal Stability and Mechanical Properties of Poly(N-(2-hydroxypropyl) methacrylamide) (PHPMA) Modified by Fe_2O_3 Nanoparticles

Noureddine Zouati[1] · **Kamel Eddine Boudraa[2,3]** · **Boumediene Lasri[2,4]**

Abstract

In this study, molecular dynamics (MD) simulation is used to investigate the effect of Fe_2O_3 nanoparticles (NPs) on the structural and thermomechanical properties of poly(N-(2-hydroxypropyl)methacrylamide) (PHPMA) nanocomposites. Five molecular models of pure PHPMA and PHPMA/Fe_2O_3 nanocomposites with different NP sizes and concentrations were constructed and analyzed. The dynamics of the various models were investigated using mean square displacement (MSD), and their glass transition temperature (T_g) was estimated using both density-temperature and MSD evaluation methods. The results reveal that the presence of Fe_2O_3 NPs enhances the molecular mobility and flexibility of polymer chains within the PHPMA matrix and decreases their T_g. Additionally, the introduction of Fe_2O_3 NPs significantly reduces the mechanical properties, such as Young's and bulk modulus, of the PHPMA polymer. Furthermore, the study demonstrates that the impact of NPs on polymer properties is strongly influenced by NP features; an increase in NP size and concentration correlates with enhanced molecular mobility and flexibility, while T_g and mechanical properties exhibit a negative correlation with these parameters. These findings offer valuable insights into the influence of Fe_2O_3 nanoparticles on the structural and thermomechanical properties of PHPMA nanocomposites, providing a foundation for optimizing their design and applications across various fields.

Keywords Poly(N-(2-hydroxypropyl)methacrylamide) (PHPMA) · Nanocomposites · Molecular dynamics simulation · Metal oxide nanoparticles

1 Introduction

In recent years, there has been a significant increase in the research and development of polymeric materials as conventional properties of these materials have become inadequate to meet the demanding requirements in various industrial

✉ Noureddine Zouati
nourreddine.zouati@univ-saida.dz

Kamel Eddine Boudraa
Boudraa.kamel@univ-saida.dz

1   Laboratory of Physicochemical Studies, University of Saida-Dr. Moulay Tahar, 20000 Saida, Algeria

2   Biology Department, Faculty of Sciences, University of Saida-Dr. Moulay Tahar, Saida, Algeria

3   Macromolecules Research Laboratory, Department of Physics, Faculty of Sciences, Abou Bekr Belkaïd University, Tlemcen, Algeria

4   Theoretical Physics Laboratory, University of Tlemcen, B.P. 230, 13000 Tlemcen, Algeria

and medical fields [1, 2]. To address this issue, new methods and technologies have been explored to modify and enhance the properties of these materials to align with their intended applications. One such approach is the use of polymer nanocomposites (PNCs) [3]. PNCs consist of a polymer matrix combined with nanoparticles, resulting in modified properties that differ from those of the individual components [4]. This is attributed to the incorporation of nanoparticles (NPs) into the polymer matrix, which has been shown through previous studies to lead to significant improvements in mechanical [5, 6], optical [7], rheological [8], thermal [9, 10], and electrical [11, 12] properties of the resulting nanocomposites. The properties of PNCs are closely related to the features of the NPs and polymer, including NP size, shape, and weight fraction, polymer molecular weight, and the type of interaction between the polymer chains and NPs [13, 14].

Molecular dynamics (MD) simulation is a powerful computational method used to study the material properties, particularly at the molecular level [15]. MD simulations can be used to predict the material properties under

different conditions, such as varying temperature and pressure [16], providing important information for the design and optimization of polymeric materials [17]. MD simulations are considered a valuable tool in material science research and development, as they can provide insights into the underlying physical and chemical processes that govern the material properties at the molecular level [18]. Wei et al. [19] employed the MD simulation to investigate the effect of nano-SiO_2 particles with different concentrations on the poly(vinyl pyrrolidone) (PVP)/polyvinyl alcohol (PVA) and observed that the incorporation of SiO_2 nanoparticles is able to modify the density, mechanical properties, and semi-crystalline character of the PVP/PVA blend systems. Wang et al. [20] studied by using MD simulation the mechanical properties and glass transition temperature (T_g) behavior of poly(ethylene terephthalate) (PET) incorporating by silica NPs and hydroxylated silica NPs, respectively. They found that the T_g of PET decreased in the presence of the silica particle and increased in the presence of hydroxylated silica, whereas the addition of hydroxyl groups on the surface of silica nanoparticles led to a more significant improvement in mechanical properties such as stiffness coefficient, compliance coefficient, Young's modulus, shear modulus, bulk modulus, and tensile strength compared to pure PET and PET/silica nanocomposite. These findings highlighted the role of interfacial interactions between PET and nanoparticles in influencing the mechanical behavior, showing stronger interfacial bonding in the PET/hydroxylated silica nanocomposite. Nematollahi et al. [21] applied MD simulation to investigate the thermal and structural properties of poly(lactic acid) (PLA)/natural rubber (NR)/SiO_2 NPs with different loading of NPs, and it was found that the interaction between the two polymer chains and the dispersion of NPs in the blend system are amounts dependent on added of NPs in the blend system. Xie et al. [22] investigated the effects of incorporating nano-SiO_2 particles with different diameters on the microstructure and thermomechanical properties of crosslinked epoxy composites using molecular dynamics simulations. The paper concludes that the presence nano-SiO_2 particles into epoxy resin effectively improved the thermal and mechanical properties, and the effectiveness was closely related to the particle size of nano-SiO_2. The T_g value increased with the decreasing particle size, while the variation of the coefficient of thermal expansion (CTE) in the glassy state demonstrated opposite trend as compared with T_g value. The mechanical properties such as Young's, shear, and bulk moduli first increased and then decreased with the decreasing particle size.

Poly(N-(2-hydroxypropyl)methacrylamide) (PHPMA) has gained significant attention in recent years due to its enhanced properties [23], biocompatibility [24], high rigidity (with a glass transition temperature of more than 350 K), low density [25], and low immunogenicity [26]. Additionally, its hydroxyl groups bond toward polar molecules [27, 28]. PHPMA has been used in a wide range of applications, including textile surface modification, photoresists, radiation curing, and paint formulations [29, 30]. Furthermore, it is one of the most suitable polymers for various applications, particularly in tissue engineering and targeted drug delivery [31, 32].

Among various types of nanoparticles, metal oxide nanoparticles, such as Fe_2O_3 iron oxide NPs, have been widely used due to their tailored chemical stability in various medium, such as water and organic solvents [33], high specific surface area [34], superparamagnetism [35], and biocompatibility [36].

When comparing the Fe_2O_3 NPs investigated in our study with commonly used nanoparticles like silica nanoparticles, it is important to consider specific application requirements and desired property enhancements. The choice between these nanoparticles depends on several factors. Fe_2O_3 NPs exhibit unique magnetic properties, providing additional functionalities to the nanocomposite system. This magnetic behavior is advantageous in applications where magnetically responsive materials are desired, such as targeted drug delivery systems or magnetic sensors [37]. On the other hand, silica nanoparticles do not respond to external magnetic fields due to their diamagnetic nature and may not offer the same level of functionality in these particular applications. The surface chemistry of the nanoparticles is crucial for their compatibility with the polymer matrix. Fe_2O_3 NPs can have varied surface chemistries depending on the synthesis methods employed, enabling tailored interactions with the polymer chains. In contrast, silica nanoparticles have a hydrophilic nature and may require additional surface modification to enhance their compatibility with hydrophobic polymer matrices like PHPMA [38]. Plichta et al. [39] prepared citrate-treated Fe_2O_3 NPs and a new PHPMA-based surface coating to guarantee minimal immunogenicity and biocompatibility and provide reactive functional groups for later chemical conjugation with a particular drug.

This study significantly contributes to a comprehensive understanding of the impact of incorporating spherical Fe_2O_3 NPs with varying NP sizes and corresponding changes in the loading level on specific PHPMA properties via molecular dynamics simulations, including polymer chain mobility, thermal stability, and mechanical properties such as Young's, shear, and bulk moduli. Lowering the glass transition temperature (T_g) of the polymer can enhance its flexibility and ductility, expanding its potential applications [40]. Likewise, a lower Young's modulus signifies a softer and more flexible material, opening up opportunities in various fields such as soft robotics, flexible electronics, medical devices, packaging, coatings, adhesives, and sealants [41].

2 Simulation Details

All MD simulations were performed using Materials Studio 7.0 software developed by BIOVIA (formerly Accelrys) [42].

2.1 Polymer Model

The selection of an appropriate chain length is a crucial factor when conducting molecular dynamics (MD) simulations of polymers. If the chain is too short, the simulation may not accurately represent real systems, while a long chain may be computationally challenging [43, 44]. To address this issue, we used the polymer and amorphous cell builder tools in Materials Studio (MS) to construct PHPMA chains with different lengths ranging from $n = 5$ to $n = 60$. We then used the solubility parameter of these pure amorphous units to determine that a chain of 40 monomers was the most suitable for our study (as shown in Fig. 1).

2.2 Fe_2O_3 Nanoparticle Model

The unit cell structure of metal oxides comes to exist with the Material Studio software. Whereof they are crystal structures provided experimentally, the lattice parameters are the experimental ones. Symmetry, space group, and lattice parameters of studied metal oxide are given in Table 1. The crystal structure of Fe_2O_3 NPs depicted in Fig. 2a was generated as spherical Fe_2O_3 NPs with different radii of 6.6 Å (Fig. 2b), 7.5 Å, 8.8 Å, and 10 Å. In order to eliminate the unsaturated boundary effect, we added a hydrogen atom to the unsaturated oxygen atoms on the surface of the Fe_2O_3 NPs, as shown in Fig. 2c.

We achieve flexibility in relative atomic positions within the nanoparticle by utilizing the "Edit Constraints" dialog. Specifically in the Materials Studio software, by unchecking the "Fix Cartesian Position" checkbox, we enable dynamic

Table 1 Symmetry, space group, and lattice parameters of studied metal oxide

Metal oxide	Space group	Symmetry	Lattice parameters	
			Lengths (Å)	Angles (degrees)
Fe_2O_3	R-3C	Hexagonal	$A = b = 5.03$, $c = 13.72$	$\alpha = \beta = 90$, $\gamma = 120$

changes in distances and angles between atoms throughout the simulation. This approach acknowledges the dynamic interactions among atoms, facilitating adjustments in their positions and orientations over time.

2.3 Polymer Nanocomposite Molecular Model

In our study, we utilized the "Construction" dialog within the amorphous cell builder in the Materials Studio software to create molecular models of pure PHPMA and PHPMA/Fe_2O_3 nanocomposites. Five models were generated, each consisting of seven PHPMA chains and one Fe_2O_3 NPs with varying nanoparticle sizes and corresponding changes in the loading level into PHPMA nanocomposites, as shown in Fig. 3. The simulated systems had an atomic number ranging from approximately 4800 to 5200, with initial density of 0.6 g/cm^3 to ensure the molecular chains had sufficient space to relax and avoid overlapping and entanglement and the periodic boundary conditions (pbc) were applied in all three principal directions. Table 2 provides a summary of the attributes of these models, including the seven PHPMA chains in each system.

2.4 MD and Annealing Simulation

We utilized the same minimizer for all initial polymer chain, Fe_2O_3 NPs and PNCs models. Our simulation incorporated
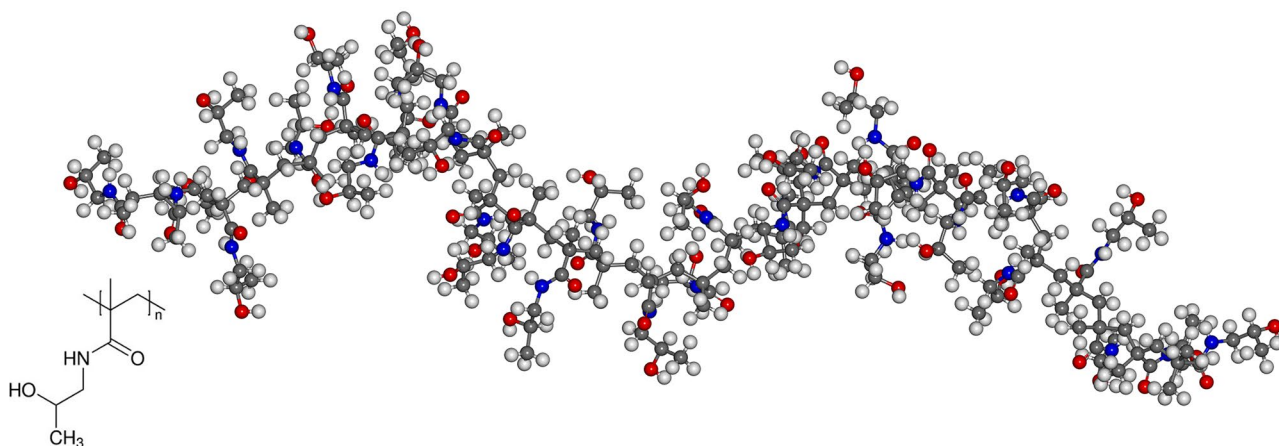

Fig. 1 Molecular model of PHPMA chain with 40 repeating units. H, white; O, red; C, gray; N, blue
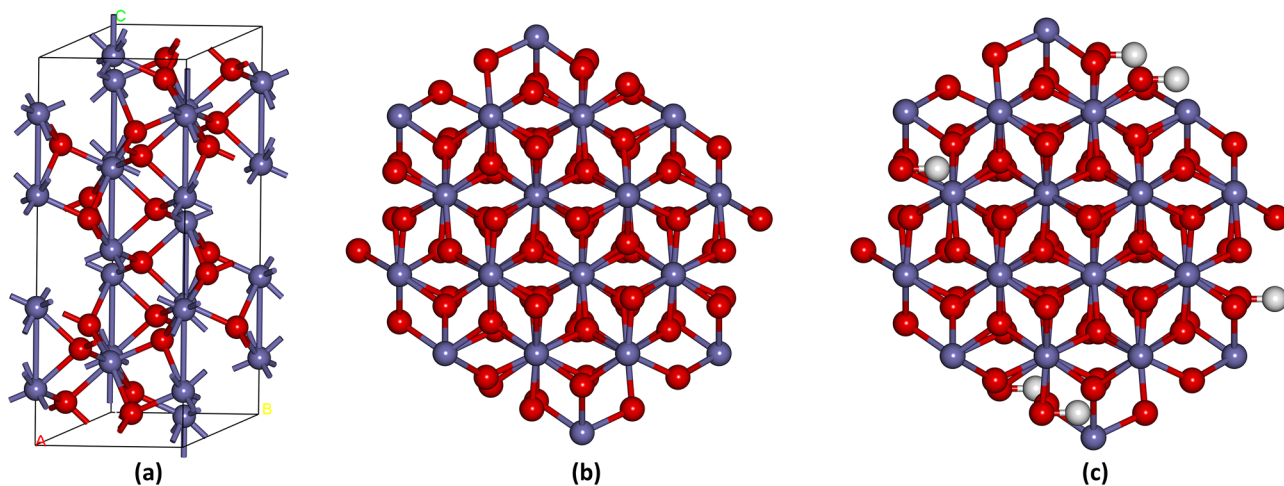
Fig. 2 Molecular models of Fe_2O_3 nanoparticle. **a** Crystal structure of Fe_2O_3 nanoparticle. **b** Spherical Fe_2O_3 nanoparticle. **c** Spherical Fe_2O_3 nanoparticle with a saturated surface. H, white; O, red; Fe, light blue

a number of advanced techniques and methods. These included using the conjugate gradient approach in the For-cite module to perform 5000 steps of energy minimization with an energy convergence threshold of 0.001 kcal/mol for all initial configurations. The simulations incorporated the DREIDING force field (FF), renowned for its effectiveness in predicting the structures and dynamics of organic, bio-logical, and main-group inorganic molecules. It employs
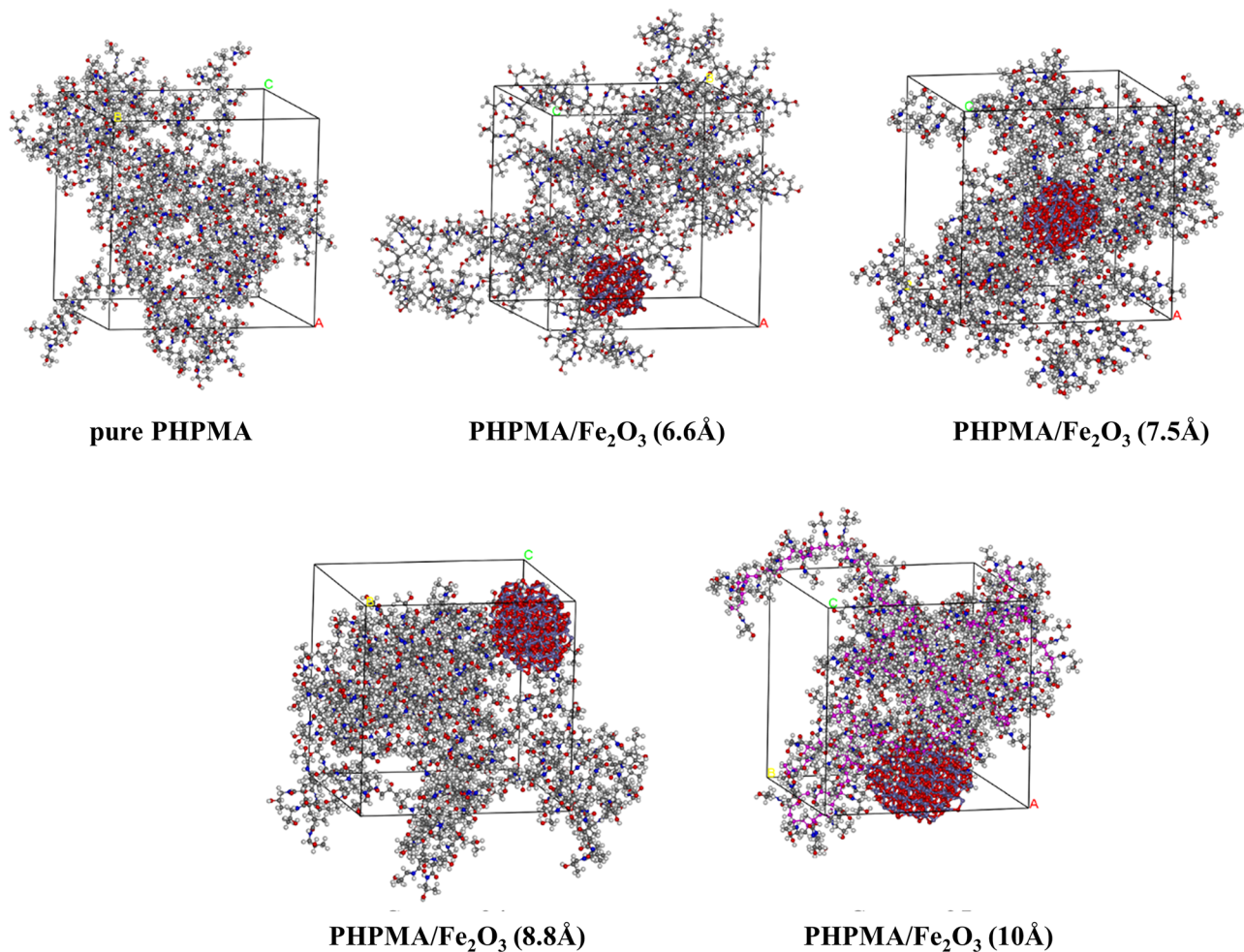

pure PHPMA

PHPMA/Fe_2O_3 (6.6Å)

PHPMA/Fe_2O_3 (7.5Å)

PHPMA/Fe_2O_3 (8.8Å)

PHPMA/Fe_2O_3 (10Å)

Fig. 3 Equilibrium models of neat PHPMA and PHPMA/Fe_2O_3 nanocomposite with different Fe_2O_3 diameters and loading

Table 2 Parameters of simulation systems

System	Cell component	Particle size (Å)	Weight fraction of component	
			PHPMA%	Fe_2O_3%
1	7PHPMA/0Fe_2O_3	Non	100	0
2	7PHPMA/1Fe_2O_3	6.6	88.9	11.1
3	7PHPMA/1Fe_2O_3	7.5	83.7	16.3
4	7PHPMA/1Fe_2O_3	8.8	77.2	22.8
5	7PHPMA/1Fe_2O_3	10	69.2	30.8

general force constants and geometry parameters derived from straightforward hybridization considerations rather than relying on individualized values dependent on the specific combination of atoms involved in bond, angle, or torsion terms [45]. Several studies found in the literature, specifically focusing on molecular dynamics simulations of polymer and PNCs, demonstrate that the DREIDING FF provides good agreement with experiments. Fereidoon et al. [46] performed systematic MD simulations (using the Material Studio software) to study the mechanical properties of both pure NPs and their hybrid PNCs using different force fields. They found that simulation results from DREIDING force field could agree with experimental data. Benkhelifa et al. explored the thermomechanical and shape memory characteristics of copolymers derived from 2-hydroxypropyl methacrylate (HPMA) and n-isobornyl acrylate (n-IBoA). Employing the DREIDING FF, their molecular dynamics simulations demonstrated a commendable concordance with experimental data [47]. The non-bonded Van der Waals and electrostatic interactions were truncated using atom-based summation approach by cutoff distance of 12.5 Å during each stage of the simulation. These measures helped to ensure the robustness and validity of our results.

To achieve the real density of each system and to release any possible tensions, we conducted a classical molecular dynamics (MD) simulation with an isothermal-isobaric ensemble (NVT and NPT) for 200 ps under NVT and 200 ps under NPT ensembles with a time step of 1 fs at a constant temperature of 298 K and pressure of 0.001 Gp (1 bar). We employed the Nose and Berendsen thermostats and barostats to control temperature and pressure. The procedure involving NVT following the NPT ensemble simulations was adopted to achieve the thermodynamic equilibrium to

properly extract converged properties [48]. Converged box sizes and corresponding system's densities as a function of NP size are presented in Table 3.

After the equilibration at 298 K, anneal simulations were performed to extract the information of mobility and glass transition temperature for each unit cell of five kinds of models. The temperature of each system was increased to 450 K, followed by a 200 ps equilibration stage at standard pressure. Then, a gradual cooling down simulation was implemented at a constant cooling rate of 25 K/100 ps, and NPT ensemble MD simulation of 100 ps was performed after each temperature decreases by 25 K until the temperature of each unit cell reached 250 K.

3 Results and Discussion

3.1 Solubility Parameter and Appropriate Chain Length

The solubility parameter is a measure of the intermolecular forces between molecules in a polymer material. It can be calculated using Eq. (1) [50]:

$$\delta = \sqrt{\frac{E_{coh}}{\nu}} = \sqrt{CED} \tag{1}$$

where ν is the mixed volume of the materials, E_{coh} represents the cohesive energy, and CED is the cohesive energy density. There is a relationship between the solubility parameter and the chain length of a polymer. As the number of repeat units increases, the solubility parameter tends to have a constant value. This suggests that when the solubility parameter value is stable, the polymer chain can accurately represent the real polymer material [50, 51]. Numerous studies have consistently affirmed the efficacy of examining changes in the solubility parameter concerning the polymer chain length to determine the minimum chain length representing the real polymer. For instance, Fu et al. [52] conducted an investigation on polyethylene terephthalate (PET) and polylactide (PLA), finding that 20 monomers serve as the shortest chain length for a real polymer. Similarly, Arenaza et al. [53] conducted a similar study, determining that the length at which the solubility parameter stabilizes represents the minimum molecular size characterizing the polymer. Their findings revealed that poly(L-lactide) (PLLA) and poly(DL-lactide) (PDLLA) reach fixed values at 20 units,

Table 3 Converged box sizes and corresponding system's densities as a function of NP size

System	Particle size (Å)	Weight fraction of Fe_2O_3%	Density (g/cm³)	Density in ref. (g/cm³)	Length (Å)
1	Non	0	1.023	1.12 [49]	36.54
2	6.6	11.1	1.075		37.39
3	7.5	16.3	1.109		37.74
4	8.8	22.8	1.169		38.11
5	10	30.8	1.191		39.27

Fig. 4 Solubility parameters vs repeat unit number
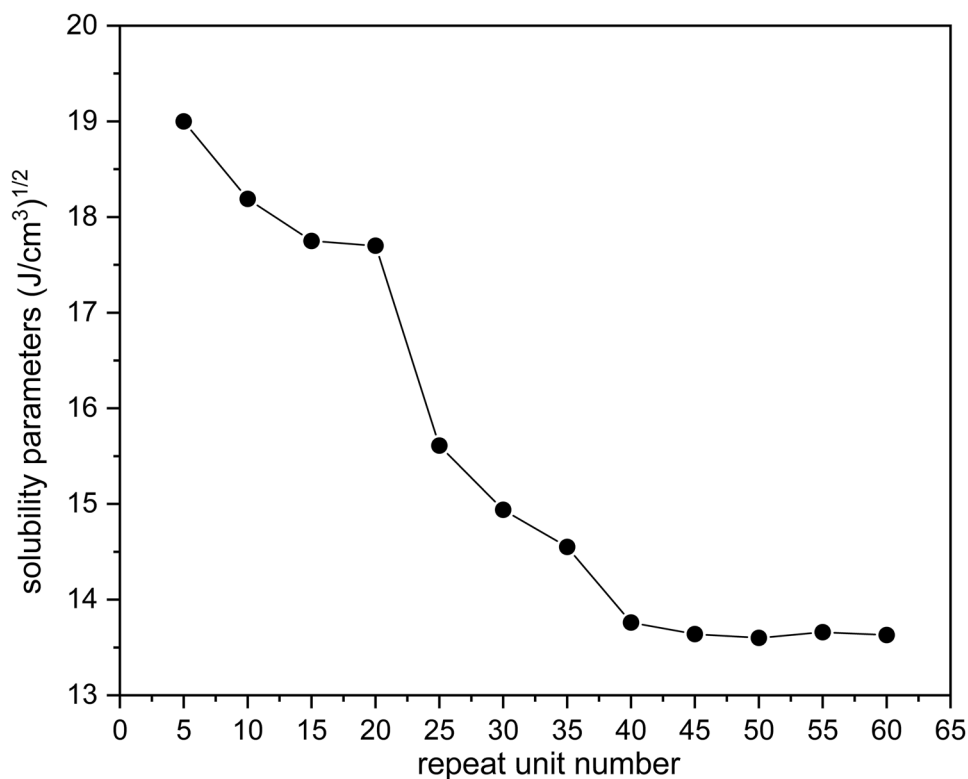
while poly(styrene) (PS) reaches 10 units. In our study, the curve depicted in Fig. 4 indicates that the solubility parameter of PHPMA becomes relatively constant when there are more than 40 repeating units. This suggests that 40 is the minimum number of repeating units required to accurately represent the PHPMA matrix in this context.

3.2 System Convergence Analysis

Regarding the PHPMA/NP mixture, the time evolution of the properties during the simulations demonstrates that the system has reached equilibrium, as indicated by the energy and temperature fluctuations falling within the

Fig. 5 Total energy, potential energy, non-bond energy, kinetic energy fluctuation, and temperature fluctuation of the final equilibrium models of PHPMA/Fe_2O_3 (6.6 Å)
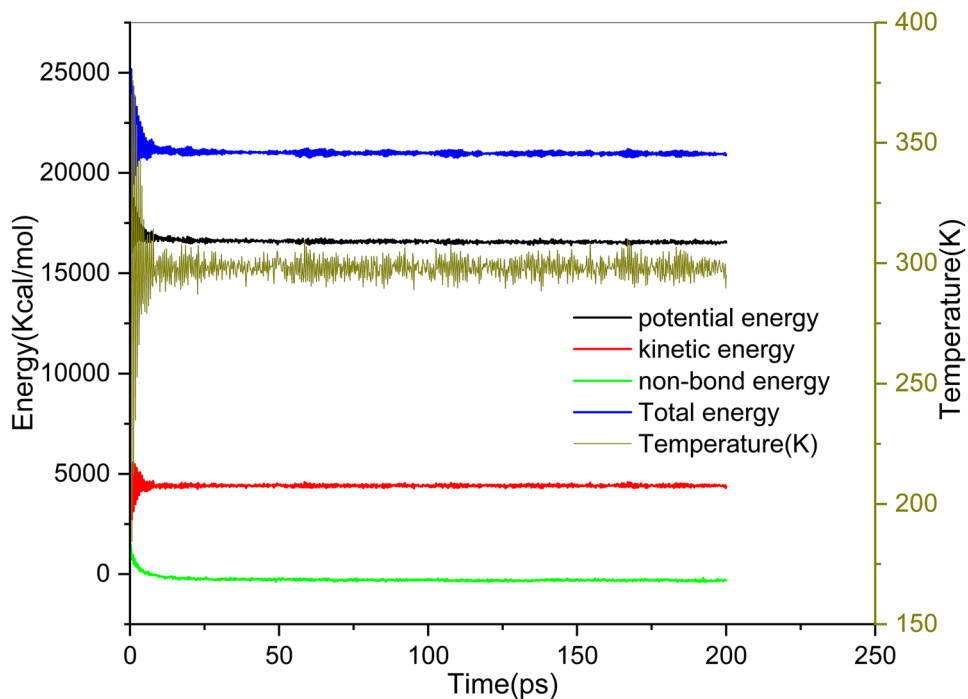
Fig. 6 Density curve observed for the NPT simulations considering the standard pressure and temperature conditions of the final equilibrium models of PHPMA/Fe$_2$O$_3$ (6.6 Å)
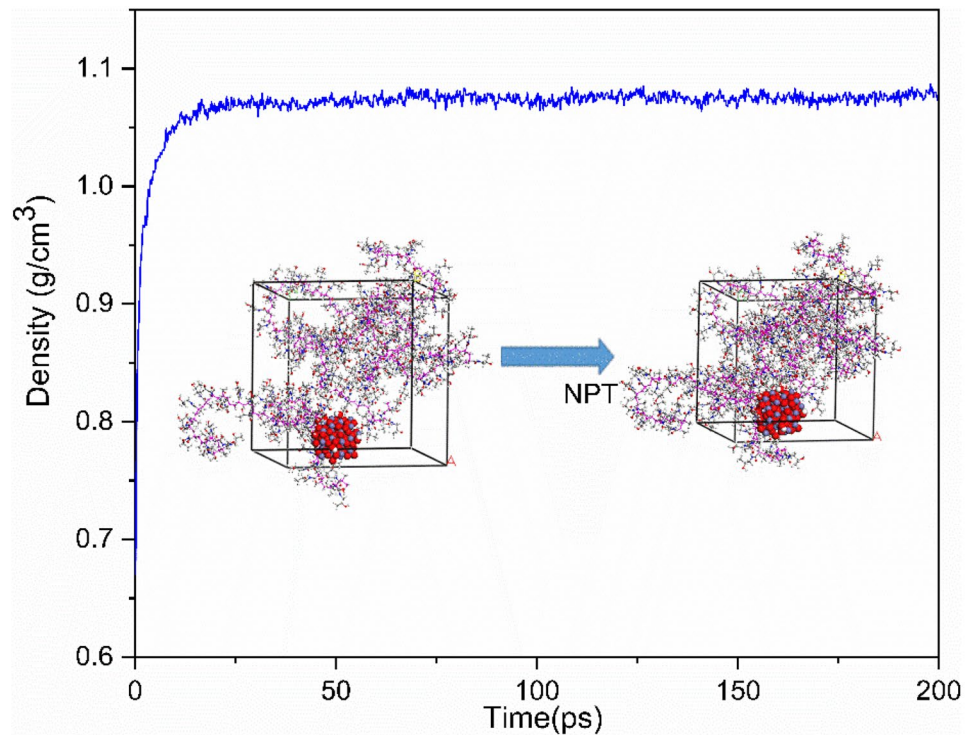
typical range of 5–10% [5–10]. This is a crucial step in the molecular dynamics simulation process, as an equilibrated system represents a stable and representative sample that can be used to accurately predict the material properties under different conditions. The observed energy and temperature fluctuations in Fig. 5 after the equilibration process confirm that the system has reached a state of equilibrium, which is essential for ensuring the validity of the

Fig. 7 MSD time evolution as a function of NP size at standard temperature and pressure
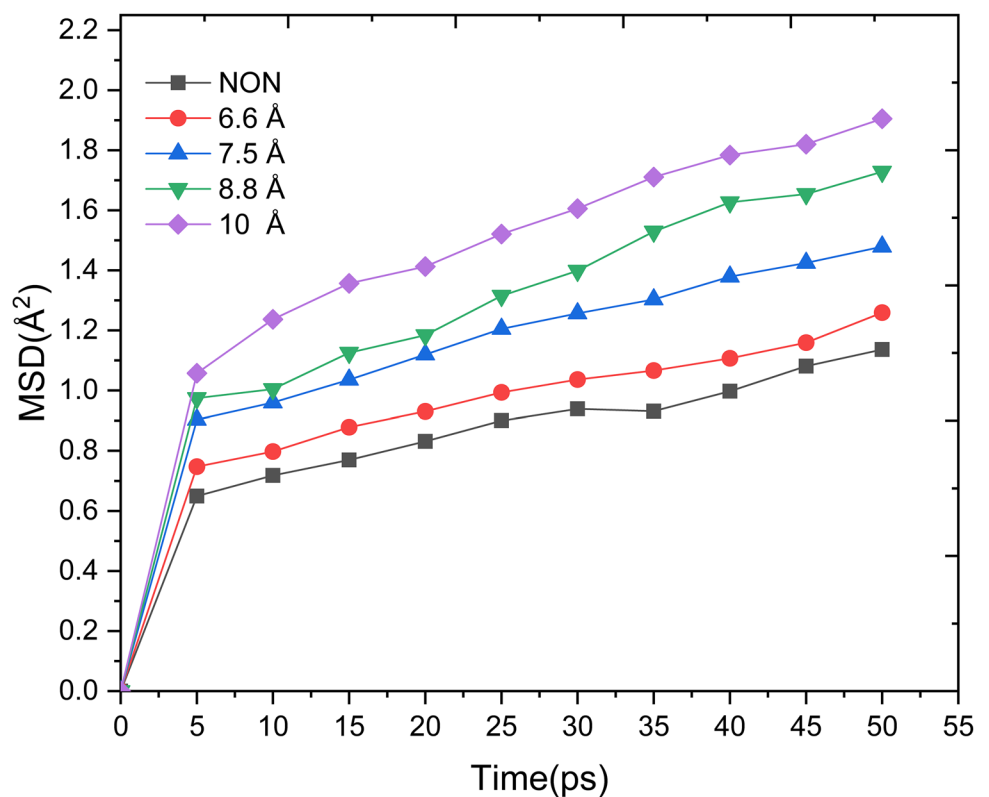
simulation results. By ensuring that the system is equilibrated, we can be confident that our simulation results are reliable and can be used to make meaningful predictions about the material properties. The equilibration process allows the system to reach a state of thermal equilibrium, where the temperature and energy are uniform throughout the system. It is evident from temperature, energy, and density curves (Figs. 5 and 6) that the simulations reached the equilibration stage, with the variations around the average oscillating within the expected range of 5–10% [54]. In addition, the simulated density of the pure polymer in this work is close to the result reported in previous research [49] presented in Table 3, verifying the reliability of the constructed models and the employed methods.

3.3 Chain Mobility

The impact of Fe_2O_3 NPs on the mobility of PHPMA chains can be investigated using mean square displacement (MSD) [55]. The MSD can be described as follows (2) [55]:

$$MSD = \frac{1}{N} \sum_{N-1}^{i=0} \left(r_i(t) - r_i(0) \right)^2 \qquad (2)$$

where N is the number of atoms in the system and $r_i(0)$ and $r_i(t)$ represent the positions of any atom i at initial time and time t, respectively. The plots of MSD time evolution as a function of NP size at standard temperature and pressure are depicted in Fig. 7. The MSD curve exhibits an increase in the presence of Fe_2O_3 NPs compared to pure (neat) PHPMA. The mean square displacement (MSD) curves exhibit a positive correlation with the size and concentration (weight fraction, loading) of Fe_2O_3 NPs. This finding suggests that the incorporation of Fe_2O_3 NPs into the PHPMA matrix significantly influences and enhances the mobility of the chains. This effect becomes more pronounced as the size and concentration of NPs increase. It is worth noting that the mobility of materials is also influenced by temperature, as depicted in Fig. 8, which shows that the dynamics of the polymer increase with increasing temperature. This trend is due to the increased thermal motion of the polymer chains. Furthermore, the variation of the MSD curves of pure PHPMA is most pronounced in the range of 260–270 K, which is associated with the glass transition temperature (T_g) of the polymer [36].

3.4 Glass Transition Temperature

The glass transition temperature (T_g) is a specific parameter of polymer materials that represents the temperature at which the polymer transitions from a rigid, glassy state to a more flexible, rubbery state, or vice versa [56]. T_g can be

Fig. 8 The variation of mean square displacement (MSD) values with ▶ time. **a** Pure PHPMA. **b** PHPMA/Fe_2O_3 (6.6 Å). **c** PHPMA/Fe_2O_3 (7.5 Å). **d** PHPMA/Fe_2O_3 (8.8 Å). **e** PHPMA/Fe_2O_3 (10 Å) at different temperatures (K)

determined using various molecular dynamics simulation methods, such as the polymer characteristics including thermal expansion, volume, thermal conductivity, and density, as well as microscopic characteristics such as polymer mobility using mean square displacement (MSD), radial distribution function (RDF), and non-bond energy [57]. In this work, the T_g of various models was estimated using density and MSD evaluation methods.

The densities of the five systems decrease linearly as the temperature increases, as shown in Fig. 9. The T_g value can be determined from the density-temperature fitting curve by finding the inflection point of each density curve through the intersection of the two linear lines that represent the transition of the amorphous polymer from the glassy state to the rubbery state, respectively. As seen in Table 4, the T_g values determined by the density-temperature fitting curve (Fig. 9) and the T_g range determined by the MSD evaluation methods (Fig. 8) are consistent with each other.

The T_g value obtained for pure PHPMA is 361.12 K, which is consistent with literature results [47]. As shown in Table 4, the T_g decreases when Fe_2O_3 nanoparticles are introduced into the PHPMA matrix, and this decreasing trend becomes more pronounced as the size and concentration of NPs increase. The incorporation of Fe_2O_3 NPs into the PHPMA matrix can disrupt the ordered structure of the polymer chains, causing the T_g of the polymer to decrease. This trend becomes more pronounced as the size and concentration of NPs increase. This phenomenon can affect the physical properties of the polymer, such as its flexibility and strength, as the T_g of a polymer can influence its modulus of elasticity.

Several researchers have focused on the relationship between the structural properties of a polymer and its glass transition temperature (T_g) [58]. As seen in Fig. 8 and Table 4, the T_g and mean square displacement (MSD) of the five systems show that the higher the MSD curve, the lower the T_g value of the polymer. This is because chain flexibility is a key factor that impacts the T_g of a polymer. The T_g tends to increase as chain flexibility decreases, so a polymer with flexible chains will often have a lower T_g. Therefore, the presence of NPs can lower the T_g of the polymer due to their ability to enhance the flexibility of the polymer chains.
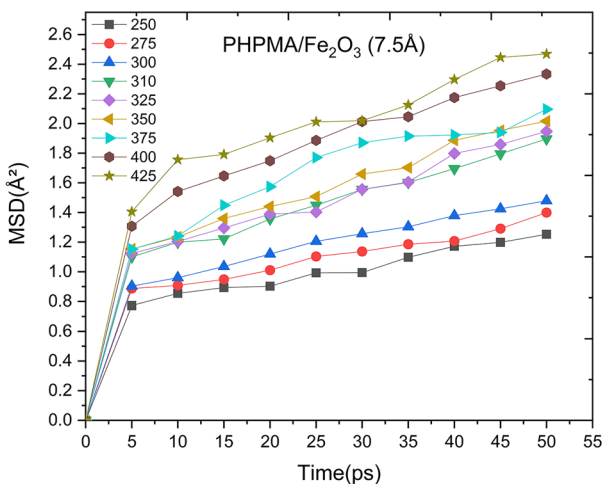
3.5 Mechanical Properties

Mechanical properties, such as Young's modulus, bulk modulus, and shear modulus, are used to indicate the rigidity of materials under different strain conditions. In this work,
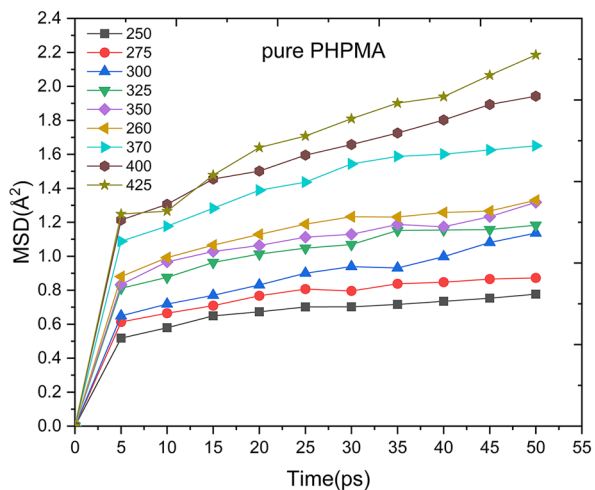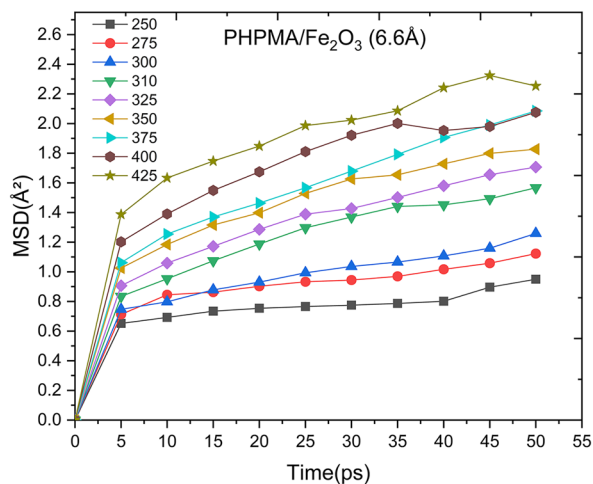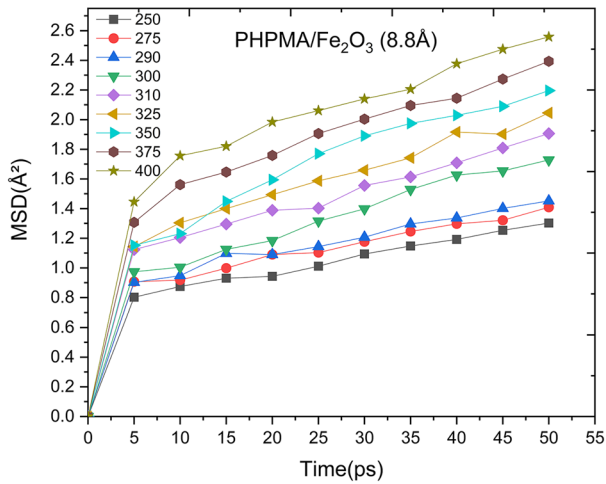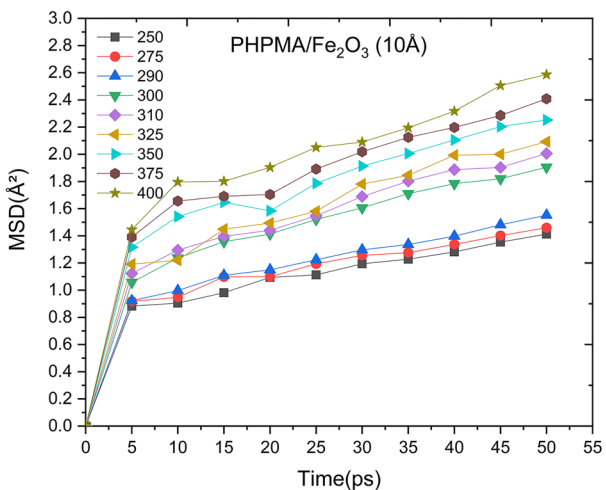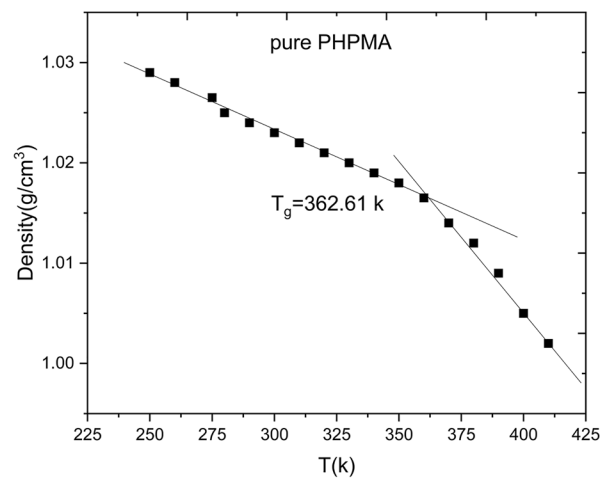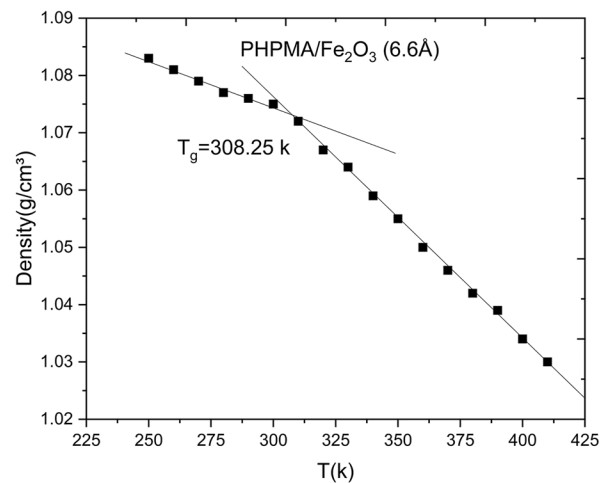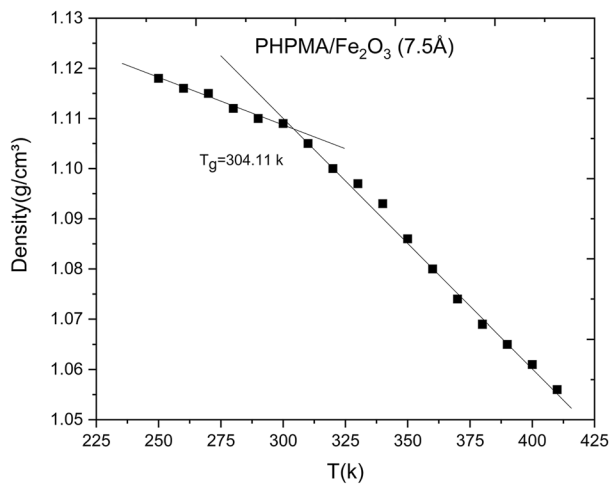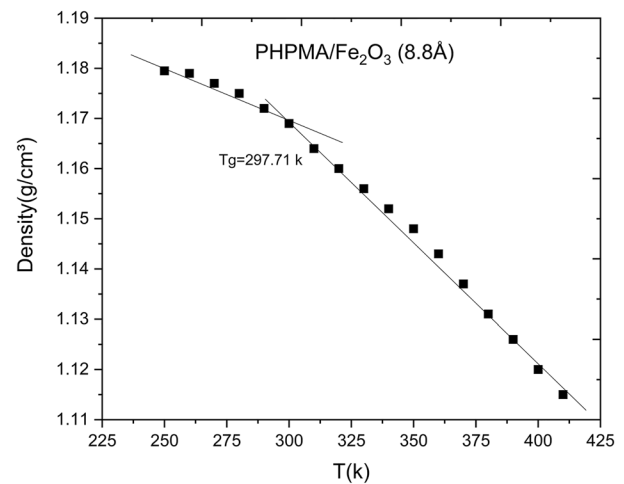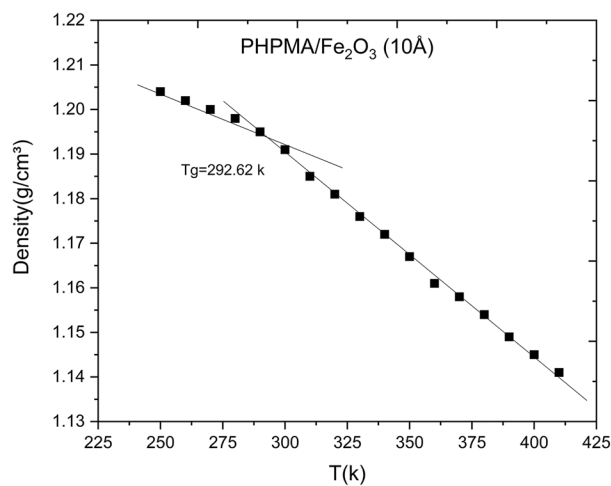
(a)

(b)

(c)

(d)

(e)

Fig. 9 Density versus temperature for **a** pure PHPMA, **b** PHPMA/Fe$_2$O$_3$ (6.6 Å), **c** PHPMA/Fe$_2$O$_3$ (7.5 Å), **d** PHPMA/Fe$_2$O$_3$ (8.8 Å), and **e** PHPMA/Fe$_2$O$_3$ (10 Å)

Table 4 T_g value of five models (units: K)

System	Particle size (Å)	T_g by fitting curve method (K)	T_g by MSD evaluation method (K)	T_g in ref. (K)
1	Non	361.12	360–370	355.15 [47]
2	6.6	308.25	300–310	
3	7.5	304.11	300–310	
4	8.8	297.71	290–300	
5	10	292.62	290–300	

the mechanical properties of the five systems were calculated using molecular dynamics (MD) simulation with the DREIDING FF based on the static stress method [59], for the equilibrium system trajectory at room temperature (300 K). The properties are shown in Fig. 10.

Figure 10 illustrates that the mechanical properties of PNC are notably different from those observed for the pure PHPMA phase. Specifically, both the Young's and the bulk moduli decrease as the size and concentration of Fe_2O_3 NPs increase. As shown in Fig. 10, the effect of Fe_2O_3 NPs with a size of 10 Å on the mechanical properties of the PHPMA nanocomposite is higher than that of the other sizes.

Based on our observations, the incorporation of Fe_2O_3 NPs into the PHPMA matrix may lead to modifications in the system's mechanical properties, specifically noticed through a decrease in the Young's and bulk moduli. This effect appears to be more pronounced as the size and weight fraction of Fe_2O_3 NPs increase. The presence of Fe_2O_3 NPs significantly improves the flexibility and molecular mobility of the chains; this can be attributed to the disruptive effect of the Fe_2O_3 NPs on the intermolecular forces within a PHPMA matrix. Nanoparticles, depending on their size, loading level, surface properties, and interaction with the polymer, can disrupt their ordered structure and create physical barriers between the polymer chains. This effect limits the close packing of polymer chains and reduces the strength of intermolecular interactions. As a result, the
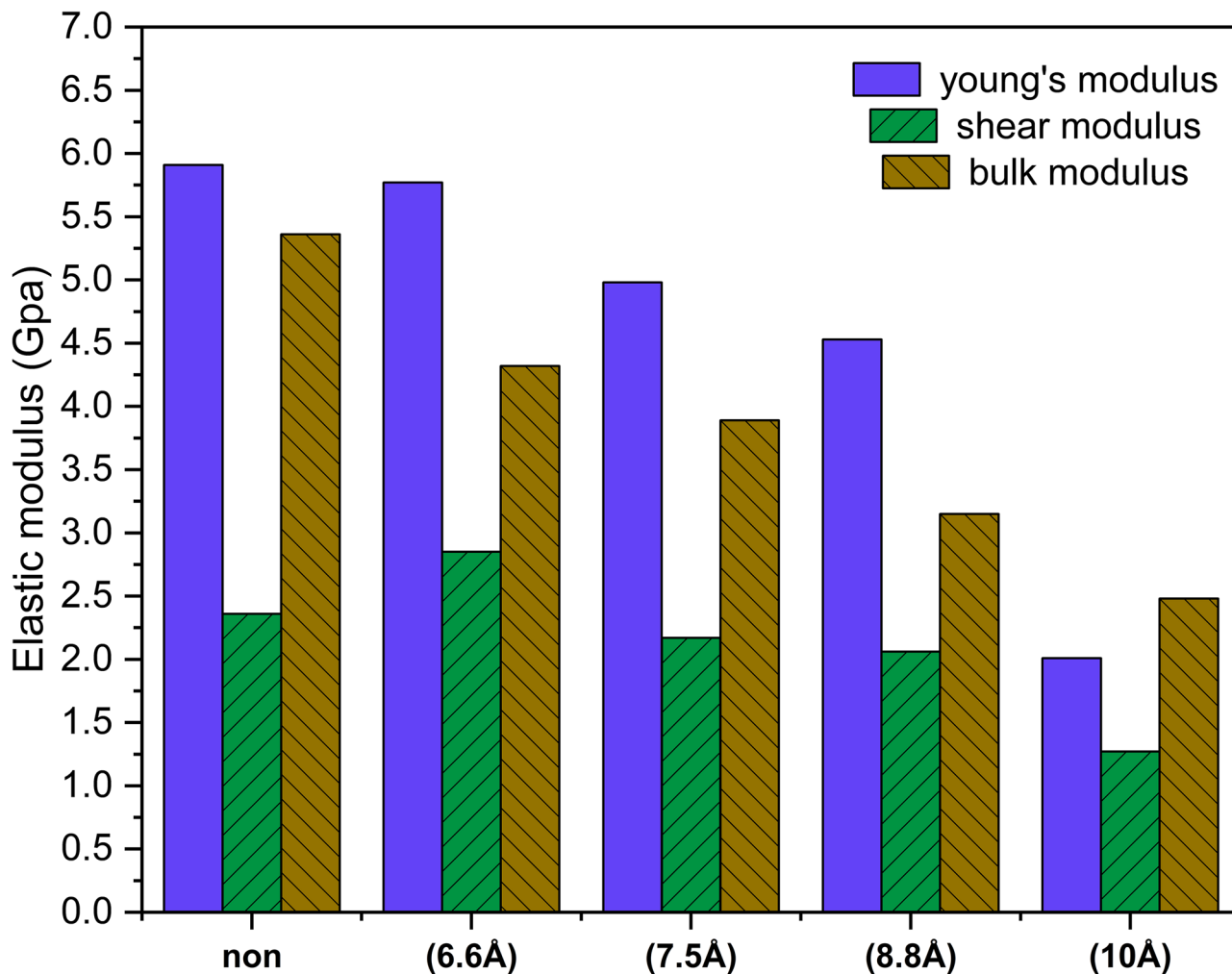

Fig. 10 The mechanical properties of five models

polymer chains gain more freedom of movement and exhibit increased flexibility and mobility. The observed relationship between higher MSD and flexibility and lower mechanical properties and rigidity of the five systems is consistent with these effects of Fe_2O_3 NPs on the polymer chains.

4 Conclusion

Molecular dynamics simulation is an effective way in analyzing and investigating the thermal and structural properties of PNCs. In this work, we applied MD simulation method to investigate the properties of pure PHPMA and PHPMA/Fe_2O_3 nanocomposites. The solubility parameters, system convergence analysis, chain mobility, glass transition temperature, and mechanical properties were studied, respectively. The simulation presented in this paper demonstrates that the incorporation of Fe_2O_3 nanoparticles (NPs) into a PHPMA polymer matrix has a significant impact on the physical properties of the material, and the presence of NPs can enhance the mobility and flexibility of the polymer chains, resulting in a reduction in the glass transition temperature (T_g) of the material. The Fe_2O_3 NPs create physical barriers between the polymer chains, inhibiting their ability to interact with one another, which leads to an increase in the mean square displacement (MSD) of the chains. In addition to these effects on the MSD and T_g of the material, the presence of Fe_2O_3 NPs can also affect the mechanical properties of the polymers. This is evident in the observed changes in the Young's and bulk moduli, which decreased significantly if compared to the pure polymer phase. The observed correlation between higher MSD and flexibility and lower mechanical properties and rigidity of the material supports these effects of Fe_2O_3 NPs on the PHPMA polymer. Overall, the incorporation of Fe_2O_3 NPs into the PHPMA polymer matrix significantly alters the physical properties of the material and has a strong impact on the mobility, flexibility, and rigidity of the polymer chains.

Declarations

Ethical Approval We wish to confirm that there are no known conflicts of interest related to this publication or substantial financial support that would have impacted the research's findings. We certify that all named authors have read, reviewed, and approved the paper and that no other individuals who meet the requirements for authorship but are not listed have contributed to the work. We also reaffirm that we all approved of the order in which the authors are listed in the manuscript. We certify that the protection of the intellectual property connected to this work has been given careful consideration and that there are no intellectual property-related obstacles to publishing, including the date of publication. By completing this, we attest to having complied with our institutions' intellectual property rules. We again reaffirm that all relevant bodies have given their ethical approval for all aspects of the research discussed in this publication. We recognize that the corresponding author including the editorial manager and any direct discussions with the office is the only point of contact for the editorial process. He is in charge of informing the other authors of his progress, their submission of corrections, and his final acceptance of the proofs. We certify that the corresponding author can access the email address we gave as being current and accurate.

References

1. A. Samir, F. Ashour, A. Hakim, M. Bassyouni, Recent advances in biodegradable polymers for sustainable applications. NPJ Mater. Degrad. **6**(1), 68 (2022). https://doi.org/10.1038/s41529-022-00277-7

2. M.S.A. Darwish, M.H. Mostafa, L.M. Al-Harbi, Polymeric nanocomposites for environmental and industrial applications. Int. J. Mol. Sci. **23**(3), 1023 (2022). https://doi.org/10.3390/ijms23031023

3. H. Wu, W.P. Fahy, S. Kim, H. Kim, N. Zhao, L. Pilato, J.H. Koo, Recent developments in polymers/polymer nanocomposites for additive manufacturing. Prog. Mater. Sci. **111**, 100638 (2020). https://doi.org/10.1016/j.pmatsci.2020.100638

4. W. Gacitua, A. Ballerini, J. Zhang, Polymer nanocomposites: synthetic and natural fillers a review. Maderas. Cienc. y Tecnol. **7**(3), 159–178 (2005). https://doi.org/10.4067/S0718-221X2005000300002

5. V.M. Bouch Er, D. Cangialosi, A. Alegría, J. Colmenero, I. Pastoriza-Santos, L.M. Liz-Marzan, Physical aging of polystyrene/gold nanocomposites and its relation to the calorimetric T g depression. Soft Matter **7**(7), 3607–36202011 (2011). https://doi.org/10.1039/C0SM01326A

6. S.P. Delcambre, R.A. Riggleman, J.J. de Pablo, P.F. Nealey, Mechanical properties of antiplasticized polymer nanostructures. Soft Matter **6**(11), 2475–2483 (2010). https://doi.org/10.1039/B926843J

7. W. Caseri, Nanocomposites of polymers and metals or semiconductors: historical background and optical properties. Macromol. Rapid Commun. **21**(11), 705–722 (2000). https://doi.org/10.1002/1521-3927(20000701)21:11%3C705::AID-MARC705%3E3.0.CO;2-3

8. M.E. Mackay, T.T. Dao, A. Tuteja, D.L. Ho, B. Van Horn, H.C. Kim, C.J. Hawker, Nanoscale effects leading to non-Einstein-like decrease in viscosity. Nat. Mater. **2**(11), 762–766 (2003). https://doi.org/10.1038/nmat999

9. C. Jiang, S. Markutsya, Y. Pikus, V.V. Tsukruk, Freely suspended nanocomposite membranes as highly sensitive sensors. Nat. Mater. **3**(10), 721–728 (2004). https://doi.org/10.1038/nmat1212

10. J. Zhu, F.M. Uhl, A.B. Morgan, C.A. Wilkie, Studies on the mechanism by which the formation of nanocomposites enhances thermal stability. Chem. Mater. **13**(12), 4649–4654 (2001). https://doi.org/10.1021/cm010451y

11. G. Polizos, E. Tuncer, A.L. Agapov, D. Stevens, A.P. Sokolov, M.K. Kidder, I. Sauers, Effect of polymer–nanoparticle interactions on the glass transition dynamics and the conductivity mechanism in polyurethane titanium dioxide nanocomposites. Polymer **53**(2), 595–603 (2012). https://doi.org/10.1016/j.polymer.2011.11.050

12. V.V. Zuev, Y.G. Ivanova, Mechanical and electrical properties of polyamide-6-based nanocomposites reinforced by fulleroid fillers. Polym. Eng. Sci. **52**(6), 1206–1211 (2012). https://doi.org/10.1002/pen.22188

13. K. Wattanakul, H. Manuspiya, N. Yanumet, Effective surface treatments for enhancing the thermal conductivity of BN-filled epoxy composite. J. Appl. Polym. Sci. **119**(6), 3234–3243 (2011). https://doi.org/10.1002/app.32889

14. Y. Zhang, S. Park, In-situ modification of nanodiamonds by mercapto-terminated silane agent for enhancing the mechanical

interfacial properties of nitrile butadiene rubber nanocomposites. Polym. Compos. **39**(10), 3472–3481 (2018). https://doi.org/10.1002/pc.24367

15. J. Lu, D. Liu, X. Yang, Y. Zhao, H. Liu, H. Tang, F. Gui, Molecular dynamics simulations of interfacial interactions between small nanoparticles during diffusion-limited aggregation. Appl. Surf. Sci. **357**, 1114–1121 (2015). https://doi.org/10.1016/j.apsusc.2015.09.142

16. J. Wang, T. Hou, Application of molecular dynamics simulations in molecular property prediction II: diffusion coefficient. J. Comput. Chem. **32**(16), 3505–3519 (2011). https://doi.org/10.1002/jcc.21939

17. C. Li, A. Strachan, Molecular scale simulations on thermoset polymers: a review. J. Polym. Sci. part B Polym. Phys. **53**(2), 103–122 (2015). https://doi.org/10.1002/polb.23489

18. H.A.L. Filipe, L.M.S. Loura, Molecular dynamics simulations: advances and applications. Mol. **27**(7), 2105 (2022). https://doi.org/10.3390/molecules27072105

19. Q. Wei, Y. Zhang, Y. Wang, M. Yang, A molecular dynamic simulation method to elucidate the interaction mechanism of nano-SiO_2 in polymer blends. J. Mater. Sci. **52**(21), 12889–12901 (2017). https://doi.org/10.1007/s10853-017-1330-0

20. Y. Wang, W. Wang, Z. Zhang, L. Xu, P. Li, Study of the glass transition temperature and the mechanical properties of PET/modified silica nanocomposite by molecular dynamics simulation. Eur. Polym. J. **75**, 36–45 (2016). https://doi.org/10.1016/j.eurpolymj.2015.11.038

21. M. Nematollahi, A. Jalali-Arani, K. Golzar, H. Modarress, Investigation of nanoparticle–polymer interaction in bio-based nanosilica-filled PLA/NR nanocomposites: molecular dynamics simulation. J. Mol. Model. **26**, 1–20 (2020). https://doi.org/10.1007/s00894-020-04431-3

22. Q. Xie, K. Fu, S. Liang, B. Liu, L. Lu, X. Yang, F. Lü, Microstructure and thermomechanical properties of crosslinked epoxy composite modified by nano-SiO_2: a molecular dynamics simulation. Polymers (Basel). **10**(7), 801 (2018). https://doi.org/10.3390/polym10070801

23. Z. Novy, V. Lobaz, M. Vlk, J. Kozempel, P. Stepanek, M. Popper, M. Petrik, Head-to-head comparison of biological behavior of biocompatible polymers poly (ethylene oxide), poly (2-ethyl-2-oxazoline) and poly [N-(2-hydroxypropyl) methacrylamide] as coating materials for hydroxyapatite nanoparticles in animal solid tumor model. Nanomater. **10**(9), 1690 (2020). https://doi.org/10.3390/nano10091690

24. X. Yang, J. Ruan, C. Ma, B. Hao, X. Huang, G. Lu, C. Feng, Synthesis and self-seeding behavior of oligo (p-phenylene vinylene)-b-poly (N-(2-hydroxypropyl) methacrylamide). Polym. Chem. **10**(34), 4718–4731 (2019). https://doi.org/10.1039/C9PY00816K

25. A. Karatza, P. Klonos, S. Pispas, A. Kyritsis, Glass transition and molecular dynamics in PHPMA-b-POEGMA block copolymers. Polymer (Guildf) **181**, 121794 (2019). https://doi.org/10.1016/j.polymer.2019.121794

26. B.S. Tucker, B.S. Sumerlin, Poly (N-(2-hydroxypropyl) methacrylamide)-based nanotherapeutics. Polym. Chem. **5**(5), 1566–1572 (2014). https://doi.org/10.1039/C3PY01279D

27. L.W. Seymour, R. Duncan, J. Strohalm, J. Kopeček, Effect of molecular weight (M w) of N-(2-hydroxypropyl) methacrylamide copolymers on body distribution and rate of excretion after subcutaneous, intraperitoneal, and intravenous administration to rats. J. Biomed. Mater. Res. **21**(11), 1341–1358 (1987). https://doi.org/10.1002/jbm.820211106

28. G. Li, M. Zhao, J. Zhang, H. Li, W. Xu, L. Pu, X. Shi, Poly (HPMA)–chlorambucil conjugate nanoparticles: facile fabrication and in vitro anti-cancer activity. New. J. Chem. 18544–18551 (2021). https://doi.org/10.1039/D1NJ03134A

29. K. Luo, J. Yang, P. Kopečková, J. Kopeček, Biodegradable multiblock poly [N-(2-hydroxypropyl) methacrylamide] via reversible addition− fragmentation chain transfer polymerization and click chemistry. Macromolecules **44**(8), 2481–2488 (2011). https://doi.org/10.1021/ma102574e

30. D. Mitra, E.-T. Kang, K.G. Neoh, Polymer-based coatings with integrated antifouling and bactericidal properties for targeted biomedical applications. ACS Appl. Polym. Mater. **3**(5), 2233–2263 (2021). https://doi.org/10.1021/acsapm.1c00125

31. R.M. Al-Nakashli, C. Cao, R. Raveendran, H. Lu, M.H. Stenzel, Increased drug-loading enhances the activity of ellipticine in poly (N-(2-hydroxypropyl) methacrylamide) PHPMA-based polymeric micelles in 2D and 3D cancer cell models. Macromol. Chem. Phys. **224**(1), 2200179 (2023). https://doi.org/10.1002/macp.202200179

32. S. Singh, 2 Polymeric biomaterials in drug-delivery systems. Polym. Biomater. Fabr. Prop. Appl., 2 (2023)

33. M. Mishra, D.-M. Chun, α-Fe_2O_3 as a photocatalytic material: a review. Appl. Catal. A Gen. **498**, 126–141 (2015). https://doi.org/10.1016/j.apcata.2015.03.023

34. G. Liu, Q. Deng, H. Wang, D.H. Ng, M. Kong, W. Cai, G. Wang, Micro/nanostructured α-Fe_2O_3 spheres: synthesis, characterization, and structurally enhanced visible-light photocatalytic activity. J. Mater. Chem. **22**(19), 9704–9713 (2012). https://doi.org/10.1039/C2JM31586F

35. A. Rahdar, H. Arabi, Preparation of super paramagnetic iron oxide nanoparticles and investigation their magnetic properties. Int. J. Sci. Eng. Invest. **1**, 10312–10313 (2012)

36. N. Ajinkya, X. Yu, P. Kaithal, H. Luo, P. Somani, S. Ramakrishna, Magnetic iron oxide nanoparticle (IONP) synthesis to applications: present and future. Materials (Basel). **13**(20), 4644 (2020). https://doi.org/10.3390/ma13204644

37. K.E. Albinali, M.M. Zagho, Y. Deng, A.A. Elzatahry, A perspective on magnetic core–shell carriers for responsive and targeted drug delivery systems. Int. J. Nanomedicine. 1707–1723 (2019)

38. M.C. Goncalves, Sol-gel silica nanoparticles in medicine: a natural choice. Design, synthesis and products. Mol. **23**(8), 2021 (2018). https://www.mdpi.com/1420-3049/23/8/2021#

39. Z. Plichta, Y. Kozak, R. Panchuk, V. Sovolova, M. Epple, L. Kobilynska, D. Horák, Cytotoxicity of doxorubicin-conjugated poly [N-(2-hydroxypropyl) methacrylamide]-modified γ-Fe2O3 nanoparticles towards human tumor cells. Beilstein J. Nanotechnol. **l9**(1), 2533–2545 (2018). https://doi.org/10.3762/bjnano.9.236

40. A.N. Frone, M.S. Popa, C.D. Usurelu, D.M. Panaitescu, A.R. Gabor, C.A. Nicolae, E. Alexandrescu, Bio-based poly (lactic acid)/poly (butylene sebacate) blends with improved toughness. **14**(19), 3998 (2022). https://www.mdpi.com/2073-4360/14/19/3998#

41. M.D. Bartlett, N. Kazem, J.M. Powell-Palm, X. Huang, W. Sun, J.A. Malen, C. Majidi, High thermal conductivity in soft elastomers with elongated liquid metal inclusions. Proc. Natl. Acad. Sci. **114**(9), 2143–2148 (2017). https://doi.org/10.1073/pnas.1616377114

42. Accelrys Inc., *Accelrys materials studio (Version 7) [Computer software]* (Accelrys Inc., San Diego, California, 2014)

43. J. Yang, X. Gong, G. Wang, Compatibility and mechanical properties of BAMO–AMMO/DIANP composites: a molecular dynamics simulation. Comput. Mater. Sci. **102**, 1–6 (2015). https://doi.org/10.1016/j.commatsci.2015.02.010

44. K. Golzar, H. Modarress, S. Amjad-Iranagh, Effect of pristine and functionalized single-and multi-walled carbon nanotubes on CO_2 separation of mixed matrix membranes based on polymers of intrinsic microporosity (PIM-1): a molecular dynamics simulation study. J. Mol. Model. **23**, 1–25 (2017). https://doi.org/10.1007/s00894-017-3436-3

45. S.L. Mayo, B.D. Olafson, W.A. Goddard, DREIDING: a generic force field for molecular simulations. J. Phys. Chem. **94**(26), 8897–8909 (1990). https://doi.org/10.1021/j100389a010

46. A. Fereidoon, S. Aleaghaee, I. Taraghi, Mechanical properties of hybrid graphene/TiO_2 (rutile) nanocomposite: a molecular dynamics simulation. Comput. Mater. Sci. **102**, 220–227 (2015). https://doi.org/10.1016/j.commatsci.2015.02.044

47. A. Benkhelifa, K.E. Boudraa, T. Bouchaour, Enhancement of shape memory properties of thermo-responsive copolymers-based 2-hydroxy propyl methacrylate and n-isobornyl acrylate. J. Therm. Anal. Calorim., 1–16 (2022). https://doi.org/10.1007/s10973-022-11532-z

48. H.J.C. Berendsen, J.P.M. van Postma, W.F. Van Gunsteren, A. DiNola, J.R. Haak, Molecular dynamics with coupling to an external bath. J. Chem. Phys. **81**(8), 3684–3690 (1984). https://doi.org/10.1063/1.448118

49. E. Yildirim, D. Cimen, A. Zengin, T. Caykara, Synthesis of poly (N-(2-hydroxypropyl) methacrylamide) brushes by interface-mediated RAFT polymerization. RSC Adv. **6**(51), 45259–45264 (2016). https://doi.org/10.1039/C6RA04189B

50. Y. Wang, Q. Wei, S. Wang, W. Chai, Y. Zhang, Structural and water diffusion of poly (acryl amide)/poly (vinyl alcohol) blend films: experiment and molecular dynamics simulations. J. Mol. Graph. Model. **71**, 40–49 (2017). https://doi.org/10.1016/j.jmgm.2016.11.001

51. J.A. Manson, L.H. Sperling, *Polymer blends and composites* (New York plenum press, New York, 1976)

52. Y. Fu, L. Liao, L. Yang, Y. Lan, Y. Mei, Y. Liu, S. Hu, Molecular dynamics and dissipative particle dynamics simulations for prediction of miscibility in polyethylene terephthalate/polylactide blends. Mol. Simul. **39**(5), 415–422 (2013). https://doi.org/10.1080/08927022.2012.738294

53. I.M. Arenaza, E. Meaurio, B. Coto, J.R. Sarasua, Molecular dynamics modelling for the analysis and prediction of miscibility in polylactide/polyvinilphenol blends. Polymer **51**(19), 4431–4438 (2010). https://doi.org/10.1016/j.polymer.2010.07.018

54. Y. Wang, Q. Wei, F. Pan, M. Yang, S. Wei, Molecular dynamics simulations for the examination of mechanical properties of hydroxyapatite/poly α-n-butyl cyanoacrylate under additive manufacturing. Biomed. Mater. Eng. **24**(1), 825–833 (2014). https://doi.org/10.3233/BME-130874

55. X. Michalet, Mean square displacement analysis of single-particle trajectories with localization error: Brownian motion in an isotropic medium. Phys. Rev. E **82**(4), 041914 (2010). https://doi.org/10.1103/PhysRevE.82.041914

56. C.-C. Huang, M.-X. Du, B.-Q. Zhang, C.-Y. Liu, Glass transition temperatures of copolymers: molecular origins of deviation from the linear relation. Macromolecules **55**(8), 3189–3200 (2022). https://doi.org/10.1021/acs.macromol.1c02287

57. M. Mohammadi, J. Davoodi, The glass transition temperature of PMMA: a molecular dynamics study and comparison of various determination methods. Eur. Polym. J. **91**, 121–133 (2017). https://doi.org/10.1016/j.eurpolymj.2017.03.056

58. K. Fu, F. Lü, Q. Xie, H. Ruan, X. Yang, S. Liang, The effects of shape and mass fraction of nano-SiO_2 on thermomechanical properties of nano-SiO_2/DGEBA/MTHPA composites: a molecular dynamics simulation study. AIP Adv. **10**(1), 015339 (2020). https://doi.org/10.1063/1.5135627

59. P.W. Tasker, The stability of ionic crystal surfaces. J. Phys. C Solid State Phys. **12**(22), 4977 (1979). https://doi.org/10.1088/0022-3719/12/22/036